EFDA–JET–PR(07)57

D. del-Castillo-Negrete, P. Mantica, V. Naulin, J.J. Rasmussen
and JET EFDA contributors

Fractional Diffusion Models of Non-Local Perturbative Transport: Numerical Tesults and Application to JET Experiments

Fractional Diffusion Models of Non-Local Perturbative Transport: Numerical Tesults and Application to JET Experiments

D. del-Castillo-Negrete[1], P. Mantica[2], V. Naulin[3], J.J. Rasmussen[3]
and JET EFDA contributors*

JET-EFDA, Culham Science Centre, OX14 3DB, Abingdon, UK

[1]Oak Ridge National Laboratory, Oak Ridge, TN 37831, USA
[2]Istituto di Fisica del Plasma Associazione Euratom-ENEA-CNR Milano, Italy
[3]Association EURATOM-RisΔ National Laboratory, Technical University of Denmark DTU, DK-4000 Roskilde, Denmark
** See annex of M.L. Watkins et al, "Overview of JET Results ", (Proc. 21 st IAEA Fusion Energy Conference, Chengdu, China (2006)).*

Preprint of Paper to be submitted for publication in
Nuclear Fusion

ABSTRACT.
Perturbative experiments in magnetically confined fusion plasmas have shown that edge cold pulses travel to the center of the device on a time scale much faster than expected on the basis of diffusive transport. An open issue is whether the observed fast pulse propagation is due to non-local transport mechanisms or if it could be explained on the basis of local transport models. To elucidate this distinction, perturbative experiments involving ICRH power modulation in addition to cold pulses have been conducted in JET for the same plasma. Local transport models have found problematic to reconcile the fast propagation of the cold pulses with the comparatively slower propagation of the heat waves generated by power modulation. In this paper, a non-local model based on the use of fractional diffusion operators is used to describe these experiments. A numerical study of the parameter dependence of the pulse speed and the amplitude and phase of the heat wave is also presented.

1. INTRODUCTION

Perturbative experiments provide valuable time dependent transport information in a relatively controlled setting that can be used to validate and test transport models. In these experiments the transient response of the plasma to externally applied small perturbations, e.g., plasma edge cooling and heating power modulation, is followed in time, see for example Ref. [1] and references therein. In the case of cold pulses, experiments in JET and other machines have shown that perturbations applied at the edge travel to the center on a time scale of a few ms, i.e. much faster than expected on the basis of diffusive time scales compatible with plasma confinement [2–6]. An open issue in describing these experiments is whether the observed fast pulse propagation is due to non-local transport mechanisms or if it could be explained on the basis of local transport models.

By local models we mean models in which the heat flux, *qd*, is determined by the Fourier-Fick's prescription

$$q_d = -\chi_d \, n\delta_x T \tag{1}$$

where we have restricted attention to transport in a one-dimensional domain, n denotes the density, and T the temperature. On the other hand, in the non-local models of interest here, the flux is given by

$$q_{nl} = -\chi_d \, n\delta_x \int K(x-y)T(y,t)dy, \tag{2}$$

where the function $K(x-y)$ accounts for the non-local contribution of the temperature at point y to the flux at point x, and the integral extends over the whole domain of the plasma. The decay of the function K measures the degree of non-locality. As expected, in the case of a Dirac delta function, $K = \delta\,(x-y)$, the local diffusive model is recovered. The local, χ_d, and non-local, χ_{nl}, diffusivities

can in general depend on x and t, and, in the non-linear case, also on T and the gradient of T. The difficulty in determining the role of non-locality versus locality in transport using cold pulse experiments is that both local and non-local models exhibit fast propagation phenomena for properly chosen model parameters and conditions. For example, fast propagation speeds can be obtained with critical temperature gradient transport models in which «d incorporates a non-linear critical threshold condition [7]. Also, non-local models of the form in Eq. (2), with algebraic decaying functions K exhibit fast pulse phenomena [8]. Thus, in order to discriminate between the two transport mechanics conclusively further experimental information is needed.

Perturbative experiments involving power modulation can provided the needed additional information. This is because cold pulses and heat waves generated from power modulation exhibit markedly different propagation properties. A promising modeling approach is then to focus on experiments in which both type of perturbations, cold pulses and power modulation, are present for the *same* plasma. These kind of experiments have been carried out in JET [4, 6], and are the main object of study in the present paper. The presence of both types of perturbations provides the necessary constrains to elucidate the role of non-locality. The general approach followed in the modeling of these experiments is to use the modulation data to calibrate (fit) the parameters of the model, and then use the model (with no free parameters left) to predict the propagation speed of the cold pulse. The attempts to follow this prescription using local transport models have not been successful [5]. In particular, as discussed in Sec. IV, local descriptions including the critical gradient model [4], the Weiland model [9], and turbulence spreading [13, 14] account reasonably well for the heat wave propagation but significantly underestimate the pulse speed. The 3-D fluid turbulence code TRB [10, 11] predicts fast propagation for both cold pulses and heat waves, and simulations using the 3-D global electromagnetic fluid turbulence code CUTIE [12, 11] are not feasible due to the long time scales involved in the power modulation experiments. The apparent lack of success of local models in reconciling the fast propagation of cold pulses with the comparatively slower propagation of heat waves observed in JET is our main motivation toexplore the use of non-local models. In particular, here we show that these experimental observations can be described using a recently proposed non-local transport model based on the use of fractional diffusion operators [8]. A preliminary version of the results presented here was discussed in Ref. [15].

The models used here are based on the use of a type of integro-differential operators known as fractional derivatives [16,17] that allow the incorporation of non-local effects in the flux. These fractional diffusion models have been successfully used to model non-diffusive test particle transport in pressure gradient driven plasma turbulence in cylindrical [18–20] and toroidal [21] geometry. In Ref. [22] a fractional Fokker-Planck equation was proposed for the kinetic description of relaxation and super-diffusive processes in turbulent electrostatic fields. In addition, it has been shown that fractional models reproduce basic non-diffusive transport phenomenology of magnetically confined fusion plasmas including anomalous scaling of confinement time in L-mode plasmas, profile peaking in the presence of off-axis fueling, pinch effects, and fast pulse propagation [8]. Pulse propagation

phenomena has also been modeled using probabilistic transport models [23, 24]. For a discussion on the connectionbetween probabilistic and fractional diffusion models see Ref. [8]. A recent review on the use of fractional diffusion to model non-diffusive transport can be found in Ref. [25].

The rest of the paper is organized as follows. The next section describes the non-local fractional transport model. Section III contains a numerical study of pulse propagation and power modulation in this model. For the cold pulses we present a numerical study on the dependence of the pulse speed on the model parameters including the diffusivity and the degree of non-locality and asymmetry. For the power modulation perturbations we present a study of the dependence of the heat wave amplitude and phase on the frequency of the modulation and the model parameters. Section IV presents the application of the model to JET data. In particular, it is shown that the model can account for both, the fast propagation of cold pulses and the relatively slow propagation of temperature perturbations caused by ICRH power modulation in the experiment. Section V contains the conclusions.

2. TRANSPORT MODEL

In this section we present a brief review of the non-local fractional diffusion model. Further details can be found in Refs. [8]. The starting point is the heat transport equation,

$$\delta_t\,[3/2nT] = -\delta_x\, q + S, \tag{3}$$

where T and n are the plasma temperature and density, q is the flux, S is the source, and x is a normalized radial coordinate. We limit attention to radial transport, and assume a onedimensional Cartesian domain, i.e. a slab approximation. In the standard diffusion model, the local Fourier-Fick's prescription in Eq. (1) is assumed to close Eq.(3). This local description assumes the existence of a well-defined transport scale and that widely separated regions of the plasma do not interact significantly with each other. From the statistical mechanics point of view, the diffusion model assumes that the underlying "microscopic" dynamics is driven by an uncorrelated, Markovian, Gaussian stochastic process, i.e. a Brownian random walk.

However, experimental, numerical, and analytical evidence has raised doubts on the validity of the restrictive assumptions upon which the standard diffusion model is based. Examples of direct numerical simulations showing non-diffusive transport include Hasegawa- Mima turbulence [26], 3-dimensional, resistive, pressure gradient-driven plasma turbulence in cylindrical [27, 19, 20] and toroidal geometry [21], and gyrokinetic plasma turbulence [28]. Non-diffusive transport has also been reported in reduced Hamiltonian models of **E×B** chaotic transport in the presence of zonal flows and drift waves [29, 30]. Experimental findings exhibiting deviations from the standard diffusion model include the anomalous scaling of the confinement time in low confinement mode plasmas [31], the non-Gaussianity of experimentally measured fluctuations [32, 33], and fast propagation phenomena in perturbative transport experiments [2, 1]. Recently, particle transport in

a toroidal plasma confinement device was shown to be nondiffusive in the presence of magnetic chaos [34]. From the analytical perspective, it has been shown that quasilinear renormalization type calculations of particle transport that avoid the restrictive localization hypothesis, lead to non-diffusive, non-local transport models of the form in Eq. (2) [35]. Also, in the presence of longrange Lagrangian velocity correlations, effective macroscopic transport models introduce non-Markovian effects [36].

The main goal of this paper is to study the role of non-locality in perturbative transport. Non-local processes are believed to play an important role in non-diffusive plasma transport in general and in the fast propagation of pulses in particular, see for example Refs. [37, 38] and references therein. Our strategy here is to use transport operators in which the local flux-gradient relation in Eq.(1) is replaced by the non-local relation in Eq.(2) according to which the flux at a given point can in principle depend on the global properties of the temperature profile. The type of non-local model is determined by the specific form of the function K. Here, following Ref. [8], we consider algebraic decaying functions of the form $K = 1/(x-y)_{\alpha}^{-1}$ and write the non-local flux as

$$q_{nl} = -\chi_d \, n\delta_x \left[l \int_a^x \frac{T(y,t)}{(x-y)^{\alpha-1}} \, dy + r \int_x^b \frac{T(y,t)}{(x-y)^{\alpha-1}} \, dy \right] , \tag{4}$$

where $1 < \alpha < 2$, l and r are constant, and χ_{nl} is the non-local diffusivity. The first term on the right hand side of Eq. (4) represents the non-local contribution of the flux at x from the plasma located to the "left" of point x ($a < y < x$) whereas the second term on the right hand side of Eq. (4) represents the contribution from the plasma to the "right" of x ($b > y > x$) where a and b are constant. The relative weight of these two terms is determined by l and r defined as

$$l = -\frac{(1-\theta)}{2\cos(\alpha\pi/2)} , \qquad r = -\frac{(1+\theta)}{2\cos(\alpha\pi/2)} , \tag{5}$$

where θ, $-1 < \theta < 1$, is the asymmetry parameter.

In principle, one could use a different function $K(x-y)$ to define the nonlocal flux. However, there are strong physical, analytical, and computational reasons to choose algebraic decaying functions. In particular, in the context of statistical mechanics, it can be shown that the fractional diffusion transport equation resulting from substituting Eq. (4) into Eq. (3) is the fluid or continuum limit of a microscopic, self-similar, non-Brownian stochastic process without a characteristic transport scale see for example [39, 19] and references therein. This has motivated the use of the non-local model in Eq.(4) to describe scale-free, self-similar turbulent transport in plasmas [19, 23, 20, 8]. From the computational point of view, the definition of the flux in terms of fractional derivatives allows the implementation of efficient, accurate, and stable finite difference numerical schemes [40, 8], which can eventually be incorporated in predictive transport codes to account for non-locality.

In Fourier space, $F[T] = \hat{T}(k) = \int e^{ikx} T(x) dx$, Eq. (4) takes the form

$$(q_{nl} = -\hat{\chi}_{nl}\, n) = -\left[\, l\,(-ik)^{\alpha-1} - r\,\widehat{(ik)^{\alpha-1}}\,\right]\hat{T}(k,t). \tag{6}$$

As expected, in the case $\alpha = 2$, and $l = r$, q_{nl} reduces to the local flux in Eq.(1). The limit $\alpha \to 1$ is less trivial but it can be shown [8] that in this case the operator on the right hand side of Eq. (4) reduces to the non-local flux used in Landau-fluid closures [41, 42]. Thus, depending on the value of α, the proposed non-local flux interpolates between the local diffusive flux and a free streaming flux. For general α, the scaling $\hat{q} \sim k^{\alpha-1}\,\hat{T}$ motivates the interpretation of the operator on the right hand side of Eq. (4) as a fractional derivative of order α. This idea can be expressed formally by introducing the integro-differential operators

$${}_aD_b^{-1}\,T = \frac{1}{\Gamma(2-\alpha)}\,\frac{\delta}{\delta x}\int_a^x \frac{T(y,t)}{(x-y)^{\alpha-1}}\,dy\,. \tag{7}$$

and

$${}_xD_b^{-1}\,T = \frac{-1}{\Gamma(2-\alpha)}\,\frac{\delta}{\delta x}\int_x^b \frac{T(y,t)}{(y-x)^{\alpha-1}}\,dy\,. \tag{8}$$

for $1 < \alpha < 2$. The operators ${}_aD_x^{\alpha-1}$ and ${}_xD_b^{\alpha-1}$ are known as the left and right Riemann- Liouville fractional derivatives of order $\alpha - 1$, and for $a = -\infty$ and $b = \infty$, their Fourier transforms satisfy [16, 17]

$$\boldsymbol{F}\,[\,{}_{-\infty}D_x^{\alpha-1} f\,] = (-ik)^{\alpha-1}\hat{f}, \qquad \boldsymbol{F}\,[\,{}_xD_{\infty}^{\alpha-1} f\,] = (ik)^{\alpha-1}\hat{f}, \tag{9}$$

As expected, for integer m, ${}_aD_x^m = (-1)^m\,{}_xD_b^m = \partial_x^m$. Using Eqs. (9), the non-local flux in Eq. (6) can be expressed in the compact form

$$q_{nl} = -\chi_{nl}\, n\,[\, l\,{}_aD_x^{\alpha-1} - r\,{}_xD_b^{\alpha-1}\,]\,T. \tag{10}$$

The parameters a and b in the integration limits define the lower and upper boundaries of the domain $x \in (a, b)$. For finite size domains, which is the case of interest here, the application of the fractional diffusion model requires the regularization of the fractional derivatives. In this paper we use the regularization ${}_aD_x^{\alpha-1}\,T \to {}_a\boldsymbol{D}_x^{\alpha-1}\,T = {}_aD_x^{\alpha-1}\,[T - T(a) - T'(a)\,(x-a)]$ and ${}_xD_b^{\alpha-1}\,T \to {}_x\boldsymbol{D}_b^{\alpha-1}\,T = {}_aD_x^{\alpha-1}\,[T - T\,(b) - T'(b)\,(b-x)]$. In the calculations presented here $x = a = 0$ corresponds to the magnetic axis, and $x = b = 1$ corresponds to the plasma boundary. For the boundary conditions we assume zero total heat flux at the magnetic axis, and fixed temperature at the edge,

$$q\,(x = 0,\, t) = [q_d + q_{nl}]\,(x = 0,\, t) = 0,\;\; T\,(x = 1,\, t) = 0. \tag{11}$$

Details on the numerical method and on the regularization of the non-local fractional operators can be found in Ref. [8].

In magnetically confined plasmas, there is a qualitative difference between core transport and edge transport. Core transport is believed to be dominated by standard, local diffusive processes, while edge transport is believed to be mostly driven by intermittent, non-diffusive processes. Motivated by this, in this paper we assume a non-local diffusivity, χ_{nl}, with a step profile of the form

$$\chi_{nl}(x) = \frac{\chi_{nl0}}{2}\left[\tanh\left(\frac{x-x_c}{L}\right) + \tanh\left(\frac{x_c}{L}\right)\right] . \qquad (12)$$

According to this expression, in the core region, $x \sim 0$, $\chi_d >> \chi_{nl}$, i.e. transport is dominated by standard diffusion. The transition to non-diffusive transport occurs at $x \sim x_c$ where there is a boundary layer of width $\sim L$ in which χ_{nl} changes from zero to the edge value χ_{nl0}. The relative value of the fractional and the standard diffusivities at the edge is quantified with the parameter $\chi_s = \chi_{nl0}/\chi_{d0}$.

3. PERTURBATIVE TRANSPORT IN THE FRACTIONAL DIFFUSION MODEL

In this section we present a numerical study of pulse propagation and power modulation in the presence of non-local transport. The results are based on the numerical integration of Eq. (3) with an $n = 1$ constant density, and a flux, $q = q_d + q_{nl}$, including the local diffusive component in Eq. (1), and the non-local component component in Eq. (10) with regularized fractional derivative operators as discussed in the previous section. The main parameters of the model are the non-locality index α, the asymmetry parameter θ, and the ratio of the magnitude of the fractional and the regular diffusivity $\chi_s = \chi_{nl}/\chi_d$. The goal is to explore the dependence on these parameters of the speed of cold pulses and of the propagation properties of "heat waves" generated by a modulating power source.

3.1. COLD PULSES

The first step in the cold pulse simulations is the computation of the steady equilibrium temperature profile, $T_0(x)$. For this we use a localized, on-axis source of the form

$$S = S_0 \exp\left(-\frac{x^2}{2\sigma_s^2}\right) \qquad (13)$$

with $\sigma_s = 0.075$. We consider two values of the non-locality parameter, $\alpha = 1.75$ and $\alpha = 1.25$. In addition, for comparison purposes, we consider the pure standard diffusive case for which $\chi_{nl} = 0$. For each value of $\pm$, we consider symmetric, $\theta = 0$, maximal asymmetric, $\theta = -1$, and asymmetric, $\theta = -0.5$, non-local operators. To explore the dependence on the ratio of the standard and fractional diffusivities we consider $\chi_s = 1$ and $\chi_s = 5$ with $x_c = 0.1$ and $L = 0.025$ in Eq. (12). As shown in Table 1, the amplitude of the heat source, S_0, was adjusted so that $T0(0) = 1$ in all cases.

Once the equilibrium profile is established, a localized cold pulse perturbation of the form

$$\delta T(x, 0) = -A \exp\left[-\frac{(x-\mu_p)^2}{2\sigma_p^2}\right], \qquad (14)$$

with $A = -0.3$, $\mu_p = 0.75$ and $\sigma_p = 0.03$ is introduced as shown in Fig.1. The evolution of the temperature perturbation, $\delta T(x, t) = T(x, t) - T_0(x)$, is obtained from the numerical integration of the fractional model with initial condition $T(x, 0) = T_0(x) + -T(x, 0)$. The main quantities of interest are the time delay, δt, and the average pulse propagation speed $V = 1/\delta t$. The time delay is defined as the time required for the core temperature to exhibit a temperature drop of size δT_c, i.e. $\delta T(0, \delta t) = \delta T_c$. The vale of the threshold δT_c is a matter of convention. Here we use $\delta T_c = -0.0375$ which corresponds to the typical value used in the analysis of the experimental data in JET that will be discussed in the next section. The normalized pulse velocity is defined as $\hat{V} = V/V_{diff}$ where V_{diff} is the pulse velocity in the diffusive case.

Figure 2 shows the spatio-temporal evolution of the perturbed temperature, $\delta T(x, t)$, and the perturbed total flux, $\delta q(x, t) = q(x, t) - q_0(x)$ (where $q_0(x)$ is the equilibrium steady state flux) for $\alpha = 1.75$ and 1.25, in the symmetric, $\theta = 0$ case with $\chi_s = 1$. For reference, the diffusive case is also included. These three numerical simulations correspond to cases 1, 2 and 3 in Table 1. In the diffusive case the pulse spreads on a diffusive time scale and the effect of the perturbation at the core is negligible. However, as the second and third columns of Fig.2 show, when the value of α is reduced, non-local transport yields a fast drop of the temperature at the core. Of particular interest is the case $\alpha = 1.25$ for which the non-local response gives rise to a temperature drop at the core larger than the drop experienced at intermediate places as evidenced by the detached "blob" observed near the core for $t \sim 0.05$. For small α the perturbed flux exhibits extended elongate areas of large positive values in the region connecting the core. These large positive flux regions are responsible for the outward temperature transport towards the edge ($x > 0$) leading to the cooling of the core. Figure 3 shows the corresponding traces of the normalized temperature perturbation $\hat{\delta T} = \delta T / |\min[\delta T(x, t_p)]|$, where $t_p = 0.01$ is the time when the pulse is introduced. At the location of the pulse, $x = 0.75$, the temperature relaxation is dominated by diffusive local transport and very similar behavior is observed independent of the value of α. However, at the core, $x = 0$, a significant delay of the signal is observed in the diffusive case. As shown in Table 1, for $\chi_s = 1$ a decrease in the value of α gives rise to an increase in the pulse speed. However, it is interesting to observe that for $\chi_s = 5$ the pulse speed for $\alpha = 1.75$ is larger than the speed for $\alpha = 1.25$, although the difference is not big.

As discussed in the previous section, the non-local contribution to the flux at a point x_0 due to the region connecting the core ($0 < x < x_0$) can in principle be different to the contribution due to the plasma in the region connecting the edge ($x_0 < x < 1$). This asymmetry depends on the parameter $\prod$ that determines the weighting factors l and r in Eq. (5). For $\theta = 0$, $l = r$ and the non-local operator is symmetric. As discussed in Ref. [8], $\theta = 0$ introduces a drift in the peak of a decaying pulse. When $\theta > 0$, $r > l$ and the drift velocity is outward (positive). On the other hand, when $\theta < 0$, $l > r$ and the drift velocity is inward (negative). However, in the fractional model an inward, i.e. negative (outward, i.e. positive) drift is always accompanied by a strongly non-local, algebraic decaying positive (negative) response [8]. Figures 4 and 5 show the dependence of the pulse dynamics on the asymmetry of the nonlocal operator. The complementary roles played by the drift and the long-range interaction

are illustrated in the temperature traces shown in Fig.5. As in Fig.3, at the location of the pulse the process is dominated by local diffusion and the three cases $\theta = 0$, $\theta = -0.5$ and $\theta = -1$ are indistinguishable from the diffusive case. However, because of the negative fractional drift, at short distances from the introduction of the pulse the fastest perturbation corresponds to $\theta = -1$ and the slowest to $\theta = 0$. Near the core the situation is exactly the opposite. Because of the non-locality, the signal corresponding to $\theta = 0$ is the fastest. As shown in Table 1, this behavior is generic, for different values of α and «s, the time delay at the core increases as θ approaches -1. Figures 6 and 7 show the dependence of the pulse dynamics on the ratio of the fractional and the standard diffusivities, $\chi_s = \chi_{nl0}/\chi_{d0}$, for fixed $\alpha = 1.25$ and $\theta = 0$. These plots, together with the results reported reported in Table 1, indicate that χ_s has a strong effect on non-local transport. In particular, for $\chi_s =$ 5 the perturbed flux exhibits an extended positive"tongue" that yields to the large outward transport responsible for the strong temperature drop at the core. Comparing the temperature traces in Fig.7 with the previous results, it is observed that the drop for $\chi_s = 5$ is about twice the size of the typical drop observed when $\chi_s = 1$, while the speed is about four times larger.

3.2 POWER MODULATION

As shown in Fig.8, in the power modulation studies we consider a source consisting of an on-axis component and an off-axis component. The on-axis term is the same as the one used in the pulse propagation studies in Eq. (13). The off-axis component includes a time-periodic amplitude modulation of the form

$$S_{oa} = \frac{S_0}{8}\,[3-\cos(2\pi\nu t)]\,\exp\left[-\frac{(x-1/2)^2}{2\sigma_{oa}^2}\right]. \qquad (15)$$

The amplitude of S_{oa} at $x = 1/2$ oscillates between the maximum value $S_0/2$ and the minimum value $S_0/4$, with a frequency ν. To study the response of the system to the power modulation we consider the perturbed temperature, $\delta T = T(x, t) - T(x)$, where $\langle T\rangle = 1/t \int_0^t T dt$ is the time averaged equilibrium profile, and write

$$\delta T(x,t) = \sum_{n=1}^{\infty} A_n(x)\cos[2\pi n\nu t + \Phi_n(x)]. \qquad (16)$$

The propagation properties of the temperature perturbation are determined by the amplitude profiles, $A_n(x)$, and the phase profiles, $\Phi_n(x)$, for the different harmonics $n = 1, 2 \ldots$. Here we focus on the $n = 1$ dominant harmonic. For the problems discussed in the section, higher order harmonics display qualitatively similar behavior.

As in the case of the pulse propagation studies, our main objective is to study the dependence of the propagation properties of δT on the parameters of the fractional diffusion model. Figure 9 shows the dependence on the non-locality parameter α. The solid lines correspond to $\alpha = 1.25$ and the dashed lines correspond to the standard diffusion case. Contrary to the dynamics of the pulse,

non-locality, as measured by the value of α, does not seem to play a prominent role in the propagation properties of the heat wave. This is particularly evident in the case of high frequency perturbations (right column of Fig.9). At low frequencies, the difference between fractional and regular diffusion is more noticeable. As expected, the propagation speed of the perturbation, as measured by the inverse of the slope of the Φ_1 profile, is larger in the fractional case. On the other hand, the damping of the perturbation at the core, as measured by the ratio $A(0)/A_{max}$, is larger in the diffusive case. The flattening of A near the core at low frequency results from $\chi_d >> \chi_{nl0}$ near $x \sim 0$ and the zero flux boundary condition. Cylindrical geometric effects, not included here, also contribute to this effect [43]. Figure 10 shows the dependence on the asymmetry parameter θ. In the high frequency case, $\nu = 57.14$, there is little difference among the three cases considered. At low frequencies, $\nu = 7.14$, the case $\nu = 1$ exhibits the least damping and slightly faster propagation speed towards the edge. Figure 11 shows the dependence of the amplitude and the phase of the temperature perturbation on the ratio of the fractional and the standard diffusivity, $\chi_s = \chi_{nl0}/\chi_d$. As in the previous cases, the differences are more evident in the low frequency regime. In general, increasing the magnitude of the non-local diffusivity, χ_{nl0}, reduces the damping and increases the propagation speed.

4. APPLICATION TO JET DATA

In this section we explore the application of the fractional diffusion model to perturbative experiments performed at JET. Several previous experiments in JET have shown that cold pulse perturbations applied at the edge, either via laser ablation of metallic impurities or shallow deuterium pellet injections, travel to the center on a time scale of a few ms, i.e. much faster than expected on the basis of diffusive time scales compatible with plasma confinement [3]. However, in those experiments it was never clarified whether such high propagation speed needed a truly non-local transport component, or if it could be explained on the basis of non-linear transport which would yield an incremental heat diffusivity, much higher than the power balance one, to account for the fast propagation of perturbations. The incremental heat diffusivity would be consistent with a turbulence driven transport mechanism in which the onset of stiff transport is regulated by a temperature critical gradient. In this description, for high levels of stiffness, very fast propagation of perturbations can be obtained, similar to the one measured for cold pulses. However, a potential problem with this approach is that such high propagation speed would characterize‘*all* types of perturbations, whilst in JET and other machines heat waves from power modulation are seen to behave consistently with a critical gradient model with a moderate level of stiffness [7].

A convincing test to discriminate between the non-local and the non-linear, critical gradient length driven, transport can be made only if the two different types of perturbations, power modulation and cold pulses, are applied to the same plasma. In this case one could derive from the power modulation heat wave analysis an estimate of the level of stiffness, and predict the speed of cold pulse propagation consistent with such level, to be compared with the experimental one, in order to decide about the need for a non-local component. These experiments have been carried out on JET

and reported in Refs. [4, 6]. Clear results have been obtained by using a very quiet plasma scenario with B_T = 3.25T, I_p = 1.6MA,q_{95} = 6.5, low density (n_{e0} = 2.7×10^{19}m^{-3}), L-mode (no ELMs), and central q above 1 in order to avoid sawteeth, so that the propagation can be followed up the plasma center. In addition to 9 MW of NBI heating, 3.7 MW of ICRH power in mode conversion scheme has been applied to heat electrons off-axis (r = 0.32) in order to expand the radius where the critical gradient is located, in order to have a significant region of plasma below threshold, implying low perturbative diffusivity and slow propagation of perturbations according to the local paradigm. In fact, in a stiff plasma all perturbations would travel very fast above threshold, according to the local value of the incremental diffusivity, and would be slowed down significantly in regions below threshold, where the turbulent diffusivity component is stabilized. In this context, there would be no asymmetry between the propagation properties of cold pulses and heat waves generated by power modulation.

Figure 12a shows the time behavior of the modulated ICRH power and of electron temperature at one spatial position, measured by a multi-channel fast ECE radiometer. The T_e time traces are then analyzed using standard Fast Fourier Transforms (FFT) according to Eq. (16), to provide spatial profiles of amplitude, A, and phase, Φ. Figure 13 shows the amplitude and phase profiles for the 1st and 3rd harmonics of the modulation frequency. The 2nd harmonic is absent because the duty-cycle of the modulation was 50%. At the end of the power modulation phase, a cold pulse is applied to cool the plasma edge. Fig.14a shows the time evolution of T_e at different radii following the edge cooling. It is observed that the signal at the core exhibits a temperature drop of 30eV in about 4 ms.

Both perturbative experiments, the cold pulse and the heat wave, have been simulated using the transport code ASTRA and the semi-empirical Critical Gradient transport Model (CGM) in Ref. [7]. Results are described in detail in [4]. The modulation shows an asymmetry in the slopes of A and Φ on the two sides of the power deposition, originated by the transition from below threshold in the core to above threshold outside the ICH deposition radius. A best fit with the CGM mode yields estimates for threshold and stiffness level. A simulation of the cold pulse using the same CGM model with the threshold and stiffness deduced from the modulation would predict a delay of the cold pulse in the core of about 22ms. Clearly, in the experiment the cold pulse is much faster, reaching the plasma core in less than 4ms. This result shows that a non local transport features needs to be invoked to explain the results of JET cold pulses. The asymmetry of behavior between power modulation and cold pulses cannot be accounted for by a local model, even when stiff transport
above threshold is taken into account.

Apart from the semi-empirical CGM model, other attempts to describe these experiments using first principle based transport models or turbulence codes have found problematic to reconcile the fast propagation of the cold pulses with the comparatively slower propagation of the heat modulation waves, as discussed in Ref. [5]. In particular, the Weiland model [9] while accounting reasonably well for the heat wave propagation, predicts a delay of the order of 50 ms for the cold pulses. The 3-D fluid turbulence code TRB [10] instead predicts a very fast cold pulse but at the same time very fast propagation of heat waves. In the 3-D global electromagnetic fluid turbulence code CUTIE [12], cold

pulses have been found to damp soon in the outer region without reaching the center, whilst power modulation simulations are not feasible due to long time scales involved in JET. Turbulence spreading models tend do a better job accounting for faster responses of the order of 18 ms, as reported in [14] whilst still maintaining good reproduction of the modulation data. However such delay is still far too long compared to experiment. This lack of success has motivated the attempt to use the above described fractional diffusion model to address the interpretation of these JET experimental results.

As it is customarily done in modeling these type of experiments, we first calibrated the fractional diffusion model by fitting the power modulation data. The source, $S(x, t) = P_0(x)+P_m(x, t)$, is taken directly from the experiment. The first term $P_0(x) = P_{OH} +P_{eNBI}+ 0.5[P_{RFmc} + P_{RFfw}]$ contains the steady state contributions from Ohmic heating, neutral beam injection, and mode conversion and fast-wave RF heating. The time modulation is of the form $P_m(x, t) = 0.5A(t)[P_{RFmc} + P_{RFfw}]$ where, as shown in Fig.12(b), $A(t)$ is a square-wave periodic function with frequency $\nu = 14.5$Hz. We assumed a constant, uniform electron density, $n = 2.6\times10^{19}$part/m^3, $\alpha = 1.25$, and a standard diffusivity profile of the form $\chi_d = (0.75 + 6x)$m^2/sec. For the fractional diffusivity we considered a profile of the form in Eq. (12) with $«_{nl}0 = 2$m$^{\alpha}$/sec.

Figure 12 compares the time evolution of the temperature perturbation in the experiment and in the fractional model at a fixed point in space. Figure 13 shows the amplitudes An and phases Φ_n of the first two dominant harmonics ($n = 1$ and $n = 3$) of the electron temperature perturbation as defined in Eq. (16). A very good agreement is observed between the fractional model and the experimental data. As mentioned before, similar levels of agreement have also been achieved using local models. However, the key issue is to be able to reproduce with the *same* parameter values and conditions the fast propagation of the pulse, something that previous models have not been able to accomplish. Figure 14 shows that the fractional model can successfully accommodate the propagation of pulses with speeds comparable to those observed in the experiment while still retaining the slower propagation of the modulation heat pulses. In particular, as Fig. 14(b) shows, the fractional model exhibits a ~30eV drop in the core temperature is about 4ms. However, it should be noted that for large times, T_e in the model exhibits a monotonic decay whereas in the experiment the evolution of T_e tends to approach a constant value. Also, the equilibrium $T_e(x)$ profile in the model tends to be flatter than in the experiment.

SUMMARY AND CONCLUSIONS

In this paper we have studied the role of non-locality on perturbative transport using a recently proposed fractional diffusion transport model. Fractional transport models are natural generalization of diffusive models that provide a unifying framework to describe non-diffusive transport including anomalous scaling and non-local/non-Markovian (memory) effects. These models have been successfully applied in the past to describe basic nondiffusive transport phenomenology in fusion plasmas, and quantitative aspects of test particle transport in plasma turbulence. Here we have shown that fractional diffusion is able to reproduce cold pulse and power modulation perturbative experiments conducted in JET that have not been satisfactorily described using local transport models.

The JET experiments discussed here show an asymmetry between the propagation of perturbations due to heat modulation and cold pulses. For $x > x_s$, where x_s denotes the location of the ICRH power deposition, waves and pulses propagate fast. However, for $x < x_s$ the heat wave slows down and is damped, but the cold pulses still travel fast. Local transport models have found problematic to simultaneously describe both types of perturbations. In particular, when these models are calibrated to reproduce the slow modulation data, they significantly underestimate the propagation speed of the pulses. Here we have shown that a transport model that incorporates a fractional diffusion non-local transport channel as well as a local diffusive channel is able to reproduce satisfactorily both the modulation data and the fast propagation of the pulses.

To complement the results of the comparison with the JET data, we have also presented a numerical study of the parameter dependence of the transport properties of the fractional model. In particular, we studied the dependence of the cold pulse speed on the degree of non-locality, α, the asymmetry of the transport process, θ, and the ratio of the fractional and the standard diffusivity χ_s. It was observed that either decreasing α or increasing χ_s leads to an increase of the propagation speed of pulses. The dependence on the asymmetry of the non-local flux is more subtle. In particular, $\theta = 0$ gives rise to a drift (whose direction depends on the sign of θ) accompanied by a long-range response in the opposite direction. The parameter dependence of the transport properties in the case of power modulation is weaker. In particular, for high frequency perturbations, the amplitude and the phase of the first harmonic of the temperature perturbation are not very sensitive to changes in α, θ, or χ_s. For low frequencies, consistent with the cold pulse results, the speed of the heat wave increases with decreasing α and increasing χ_d. In experiments and numerical simulations, the phase profile Φ exhibits an asymmetry with respect to $x = x_s$ which gives rise to different inward and outward heat wave propagation speeds. In the critical gradient model this type of asymmetry results from the threshold condition. In the model discussed here (which does not includes a critical gradient threshold) the asymmetry results from the interplay of non-local effects, boundary conditions, and the built-in asymmetry incorporated by the prescribed diffusivity profiles, χ_{nl} and χ_d.

Non-locality and critical gradient non-linearities play a complimentary role, and a complete model of perturbative transport most likely should include both. The incorporation of a critical threshold gradient condition in the diffusivity χ_{nl} of the fractional model is formally straightforward, although it is numerically nontrivial. The main motivation to limit attention in this paper to linear non-local models without critical gradients is conceptual and mathematical simplicity. The relatively simple linear model discussed here, has allowed us to make evident the crucial, and previously overlooked role played by non-locality, independent of further potential complications due to nonlinearity. However, to make further progress it would be of interest to solve the fractional diffusion model incorporating a critical gradient condition.

ACKNOWLEDGMENTS

This work was sponsored by the Oak Ridge National Laboratory, managed by UTBattelle, LLC,

for the U.S. Department of Energy under contract DE-AC05-00OR22725. This work was carried out within the framework of the European Fusion Development Agreement. The views and opinions expressed herein do not necessarily reflect those of the European Commission.

REFERENCES

[1]. P. Mantica and F. Ryter, C.R. Physique **7**, 634-649 (2007).
[2]. K. W. Gentle, G. Cima, H. Gasquet, G.A. Hallock, et al., Phys. Plasmas **2**, 2292 (1995).
[3]. P. Galli et al., Nucl. Fusion, Vol. **38**, No. 9 (1998).
[4]. P. Mantica et al., Proc.19th Intern. Conf. on Fusion Energy, Lyon [IAEA, Vienna,2002] EX/P1-04.
[5]. P.Mantica et al., Fast core response to edge cooling in JET:experiments and modeling, oral presentation at 11th EU-US Transport Task Force Workshop, Marseille, France, 2006, http://www-fusion-magnetique.cea.fr/ttf2006/prog/drafts/025.pdf
[6]. P. Mantica et al., "Core transport studies in JET". Accepted for publication in FS & T (2008).
[7]. Garbet, Plasma Phys. Control. Fusion **46** (2004) 13511373
[8]. D. del-Castillo-Negrete, Phys. Plasmas **13**, 082308 (2006).
[9]. H. Nordman, J.Weiland and A.Jarmen, Nucl. Fusion **30**, 983 (1990).
[10]. X. Garbet, et al., Phys. Plasmas **8**, 2793 (2001).
[11]. L. Garzotti, et al., Nucl. Fusion **46**, 73-81 (2006).
[12]. A. Thyagaraja, et al., Eur. Journ. Mech B/Fluids/B **23**, 475 (2004).
[13]. Naulin V, Nielsen AH, Rasmussen JJ Phys. Plasmas **12** (122306 (2005).
[14]. J.J. Rasmussen et al., 33rd EPS Conf. on Plasma Phys. Rome, June 2006 ECA Vol.30I, P-1.076 (2006)
[15]. D. del-Castillo-Negrete, et al., 34rd EPS Conf. on Plasma Phys. O4.003Warsaw, Poland, June 2007
[16]. S. G. Samko, A. A. Kilbas, and O. I. Marichev, *Fractional Integrals and Derivatives*, (Gordon and Breach Science Publishers, Amsterdam, 1993).
[17]. I. Podlubny, *Fractional Differential Equations* (Academic Press, San Diego, 1999).
[18]. D. del-Castillo-Negrete, B. A. Carreras, and V. Lynch, 2004: Proc. 20th Intern. Conf. on Fusion Energy, Villamora [IAEA, Vienna, 2004] TH/1-2.
[19]. D. del-Castillo-Negrete, B. A. Carreras, and V. E. Lynch, Phys. Plasmas **11**, 3854 (2004).
[20]. D. del-Castillo-Negrete, B. A. Carreras, and V. E. Lynch, Phys. Rev. Lett., **94**, 065003 (2005).
[21]. L. Garcia L, B. A. Carreras, Phys. of Plasmas, **13** (2), (2006).
[22]. A.V. Chechkin, and V. Yu. Gonchar, Phys. of Plasmas **9** (78), (2002).
[23]. B. Ph. van Milligen, R. Sanchez, and B. A. Carreras, Phys. Plasmas **11** 2272 (2004).
[24]. B. Ph. van Milligen, B. A. Carreras, V. E. Lynch, and R. Sanchez, Nucl. Fusion **47** 189-195 (2007).
[25]. D. del-Castillo-Negrete, "Fractional diffusion models of anomalous transport", in: R. Klages, G. Radons, I. M. Sokolov (Eds.), *Anomalous Transport* (Wiley-VCH, Weinheim, 2008).
[26]. S.V. Annibaldi, G. Manfredi, and R.O. Dendy, Phys. of Plasmas **9** (3): 791-799 (2002).

[27]. B.A. Carreras, V.E. Lynch V.E., and G. M.. Zaslavsky, Phys. of Plasmas **8** (12) 5096- 5103 (2001).
[28]. T. Hauff, F. Jenko, and S. Eule Phys. Plasmas **14**, 102316(2007)
[29]. D. del-Castillo-Negrete, Phys. Fluids **10**, 576 (1998).
[30]. D. del-Castillo-Negrete, Phys. Plasmas **7**, 1702 (2000).
[31]. R. J. Goldstone. Plasma Phys. Controlled Fusion **26**, 87 (1984).
[32]. R. Jha, P. K. Kaw, D.R. Kulkami, J. C. Parikh, and the ADITYA Team, Phys. Plasmas **10**, 699 (2003).
[33]. V. Yu. Gonchar, et al., Plasma Phys. Rep. **29**, 380 (2003).
[34]. G. Spizzo, R.B. White, and S. Cappello Phys. Plasmas **14**, 102310(2007)
[35]. R. Sanchez, B.A. Carreras, D.E. Newman, V.E. Lynch, and B.Ph. van Milligen, Phys.Rev. E **74**, 016305 (2006).
[36]. R. Balescu, Phys. Rev. E **51**, 5, 4807 (1995).
[37]. J.D. Callen, and M.W. Kissick. Plasma Phys. Controlled Fusion **39**, B173 (1997).
[38]. A. Yoshizawa, S. I. Itoh, and K. Itoh, *Plasma and Fluid Turbulence*, (Institute of Physics, Series in Plasma Physics, 2003).
[39]. R. Metzler, and J. Klafter, Phys. Rep., **339**, 1, (2000).
[40]. V. Lynch, B.A. Carreras, D. del-Castillo-Negrete, K.M. Ferreira-Mejias, and H.R. Hicks, J. Comput. Phys. **192**, 406-421 (2003).
[41]. G.W. Hammett, and F. W.Perkins. Phys. Rev. Lett., **64**, 25 (1990).
[42]. E.D. Held, J.D. Callen, C.C. Hegna, and C. R. Sovinec, Phys. Plasmas **8**, 1171 (2001).
[43]. Jacchia, A., et al., Phys. Fluids B**3**, 3037 (1991).

Case	S_0	α	θ	χ_s	δt	V	$\hat{V}$
1	11.48	diffusive	diffusive	1	0.0916	10.9	1.0
7	22.04	1.75	-1	1	0.0474	21.1	1.9
5	33.14	1.25	-1	1	0.0457	21.9	2.0
8	19.55	1.75	-0.5	1	0.0293	34.1	3.1
4	27.92	1.25	-0.5	1	0.0183	54.6	5.0
9	133.56	1.25	-1	5	0.0171	58.5	5.4
10	62.76	1.75	-1	5	0.0161	62.1	5.7
2	16.98	1.75	0	1	0.0145	69.0	6.3
11	50.67	diffusive	diffusive	5	0.0144	69.4	6.4
3	22.48	1.25	0	1	0.0095	105.3	9.6
12	103.78	1.25	-0.5	5	0.0066	151.5	13.9
13	51.31	1.75	-0.5	5	0.0061	163.9	15.0
6	74.96	1.25	0	5	0.0042	238.1	21.8
14	39.18	1.75	0	5	0.0038	263.2	24.1

Table 1: Summarizing the dependence of the cold pulse speed V, normalized speed $\hat{V}$, and time delay of the pulse δt, on the fractional model parameters α, θ and χ_s, and the magnitude of the external source S_0.

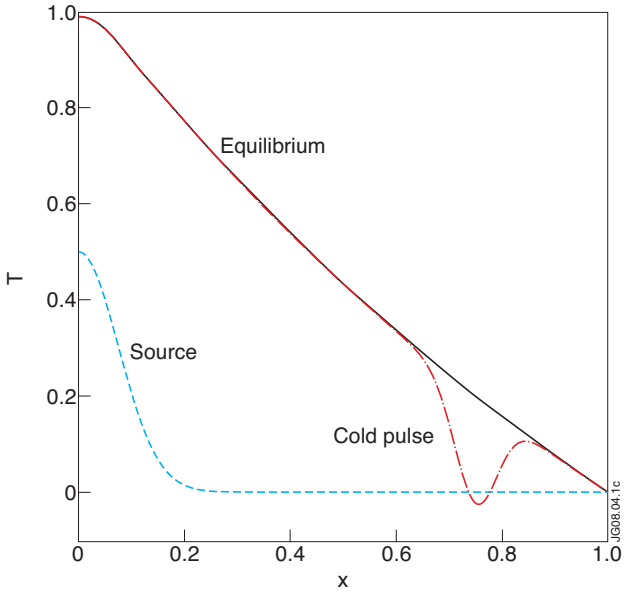

Figure 1: In the cold pulse perturbation numerical studies, a monotonically decreasing temperature profile resulting from an on-axis source is perturbed at the edge as shown in the diagram. The magnitude of the source is adjusted as shown in Table 1 so that for all the values considered of the model parameters α, θ and χ_s, the central temperature remained fixed at T(0) = 1.

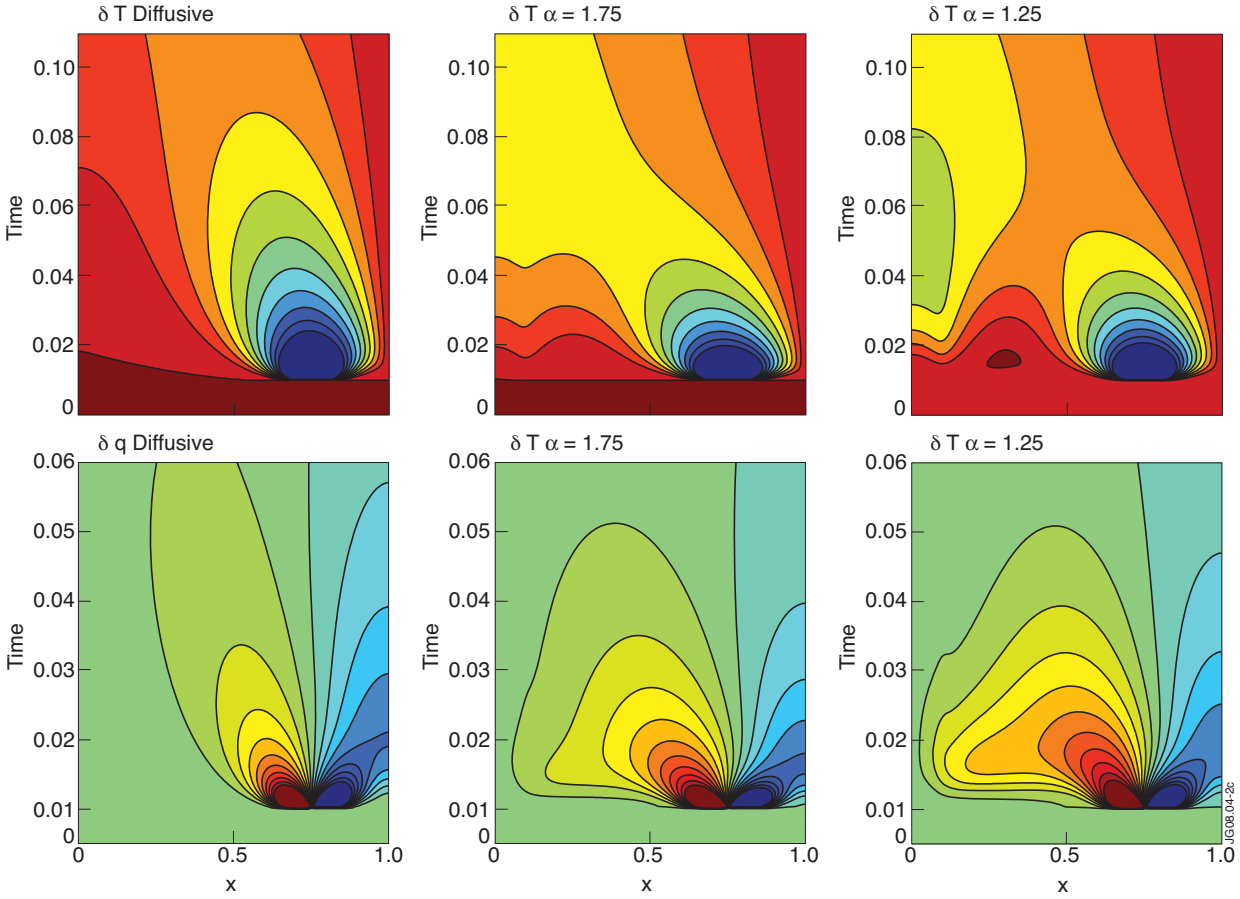

Figure 2: Dependence of the evolution of the cold pulse on the non-locality parameter α for θ = 0 and χ_s = 1. The three columns correspond to cases 1, 2, and 3 in Table 1. The top three contour plots show the spatio-temporal evolution of the perturbed temperature $\delta T = T(x, t) - T_0(x)$ with dark blue corresponding to the minimum of δT , and dark red corresponding to δT = 0. The bottom three panels show the corresponding perturbed flux $\delta q = q(x, t) - q0(x)$ with dark blue denoting large negative values and dark red denoting large positive values. The first column corresponds to the standard diffusive model. Figure 3 shows the corresponding temperature traces.

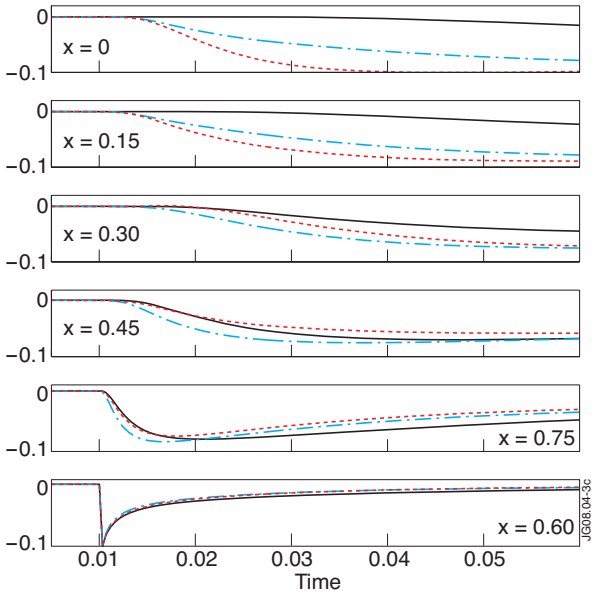

Figure 3: Traces of normalized temperature perturbation $\delta\hat{T} = \delta T/|min[\delta T\ (x, 0.01)]|$ at various spatial locations corresponding to the simulations shown in Fig.2 with $\theta = 0$ and $\chi_s = 1$ and $\alpha = 1.75$ (blue curve) and $\alpha = 1.25$ (red curve). The black curve corresponds to the standard diffusive result.These three cases correspond to cases 1, 2, and 3 in Table 1 respectively.

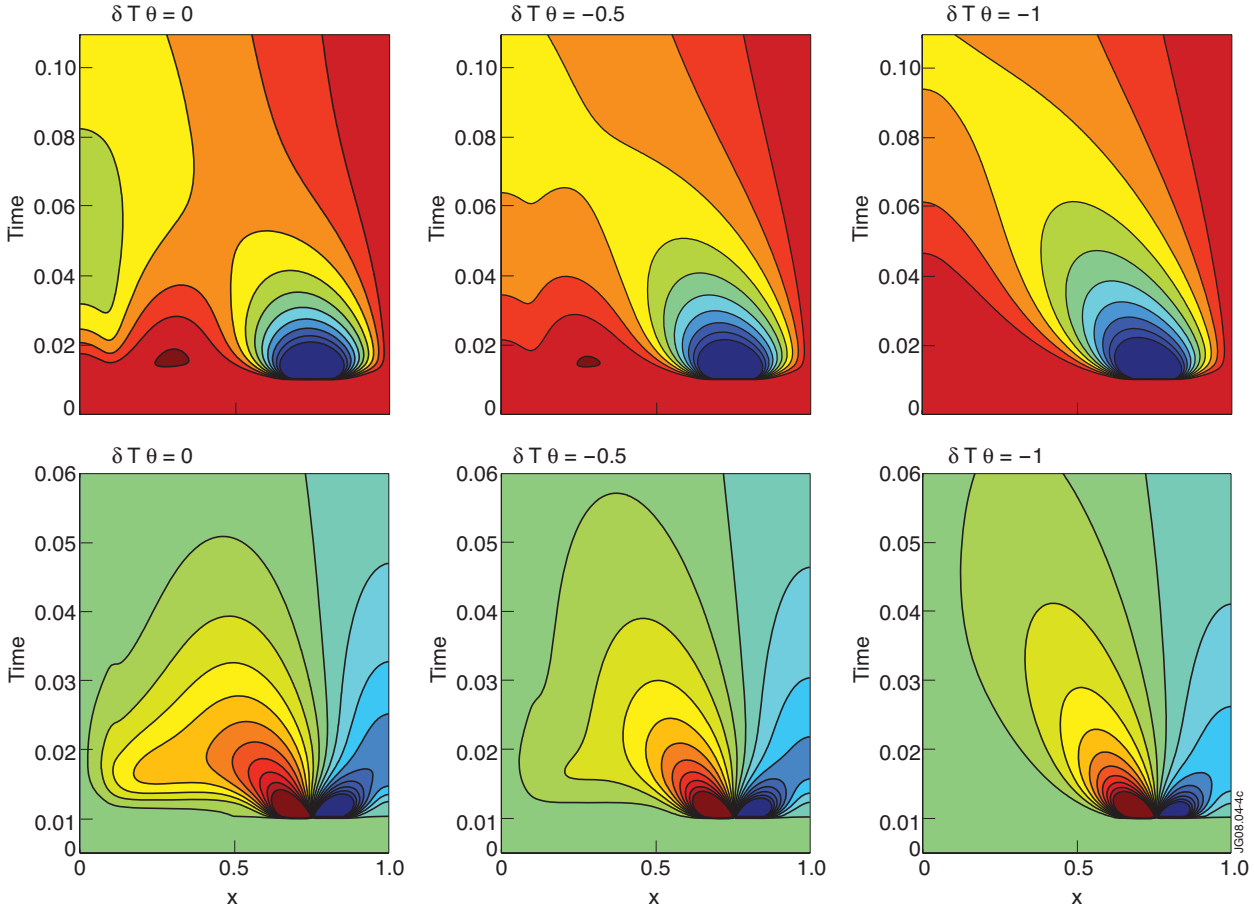

Figure 4: Dependence of the evolution of the cold pulse on the asymmetry parameter θ for $\alpha = 1.25$ and $\chi_s = 1$. The three columns correspond to cases 3, 4, and 5 in Table 1. The top three contour plots show the spatio-temporal evolution of the perturbed temperature $\delta T = T(x, t) - T_0(x)$ with dark blue corresponding to the minimum of ´T and dark red corresponding to $\delta T = 0$. The bottom three panels show the perturbed flux $\delta q = q(x, t) - q0(x)$ with dark blue denoting large negative values and dark red denoting large positive values. The case $\theta = 0$ corresponds to the symmetric case, $\theta = -1$ to the extremal asymmetric case, and $\theta = -0.5$ to an intermediate asymmetric case. Figure 5 shows the corresponding temperature traces including the standard diffusive case for reference.

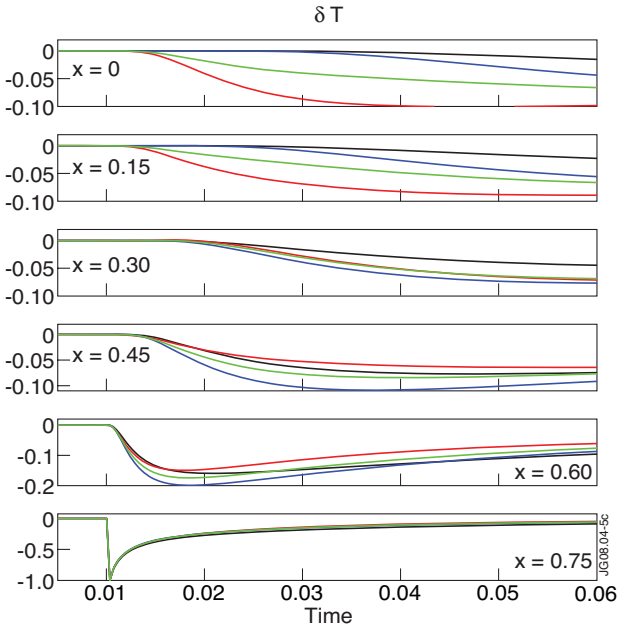

Figure 5: Traces of normalized temperature perturbation δT at various spatial locations corresponding to the cases shown in Fig. 4 with $\alpha = 1.25$, $\chi_s = 1$ and $\theta = 0$ (red curve), $\theta = -0.5$ (green curve), and $\theta = -1$ (blue curve). These three cases correspond to cases 3, 4, and 5 in Table 1 respectively. For reference, the standard diffusive case is shown in black.

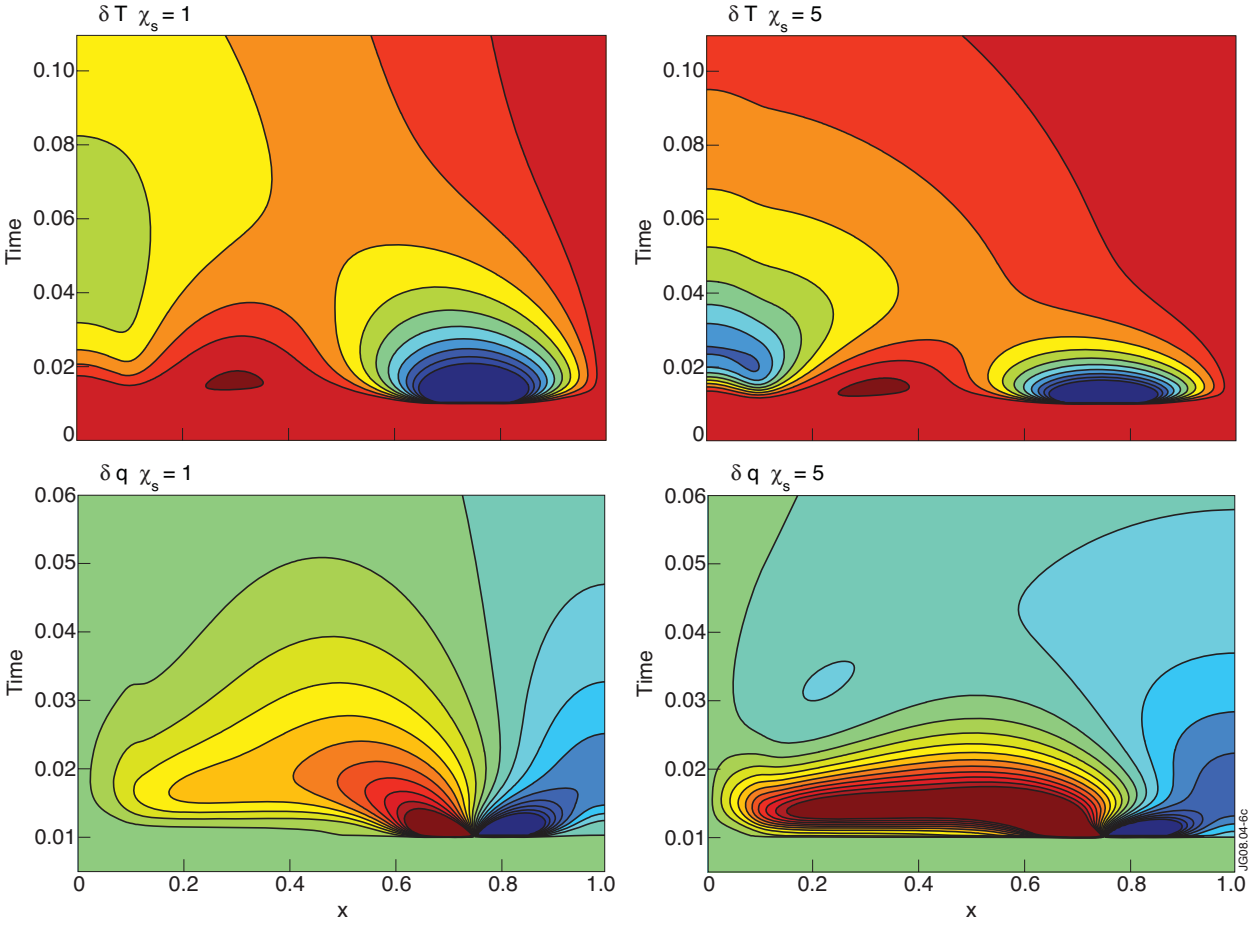

Figure 6: Dependence of the evolution of the cold pulse on the parameter χ_s for $\theta = 0$ and $\alpha = 1.25$. The two columns correspond to cases 3, and 6 in Table 1.The top two contour plots show the spatio-temporal evolution of the perturbed temperature $\delta T = T(x, t) - T_0(x)$ with dark blue corresponding to the minimum of δT and dark red corresponding to $\delta T = 0$. The bottom two panels show the perturbed flux $\delta q = q(x, t) - q_0(x)$ with dark blue denoting large negative values and dark red denoting large positive values. Figure 7 shows the corresponding temperature traces.

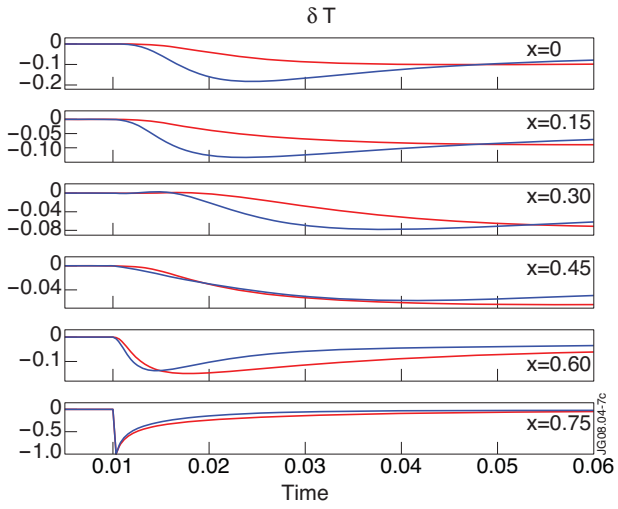

Figure 7: Traces of normalized temperature perturbation δT at various spatial locations corresponding to the cases shown in Fig.6 with $\alpha = 1.25$, $\theta = 0$ and $\chi_s = 1$ (red curve) and $\chi_s = 5$ (blue curve). These two cases correspond to cases 3, and 6 in Table 1 respectively.

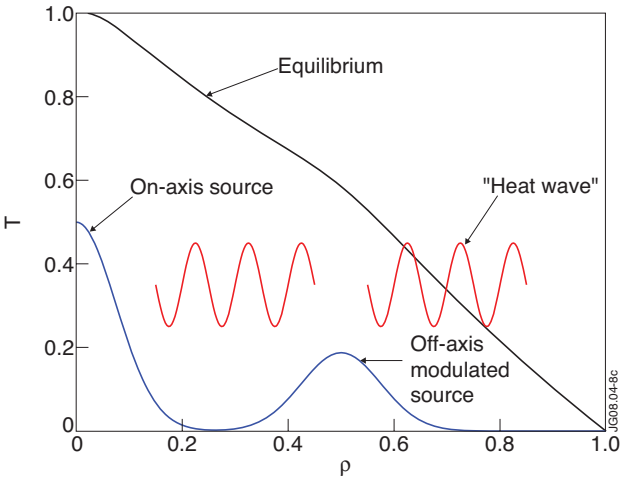

Figure 8: In the power modulation numerical studies, a monotonically decreasing temperature profile resulting from an on-axis source was perturbed by a modulated off-axis source. The magnitude of the sources was adjusted so that, in the absence of modulation, the central temperature remained fixed at T(0) = 1 for all the values considered of the model parameters α, θ and χ_s.

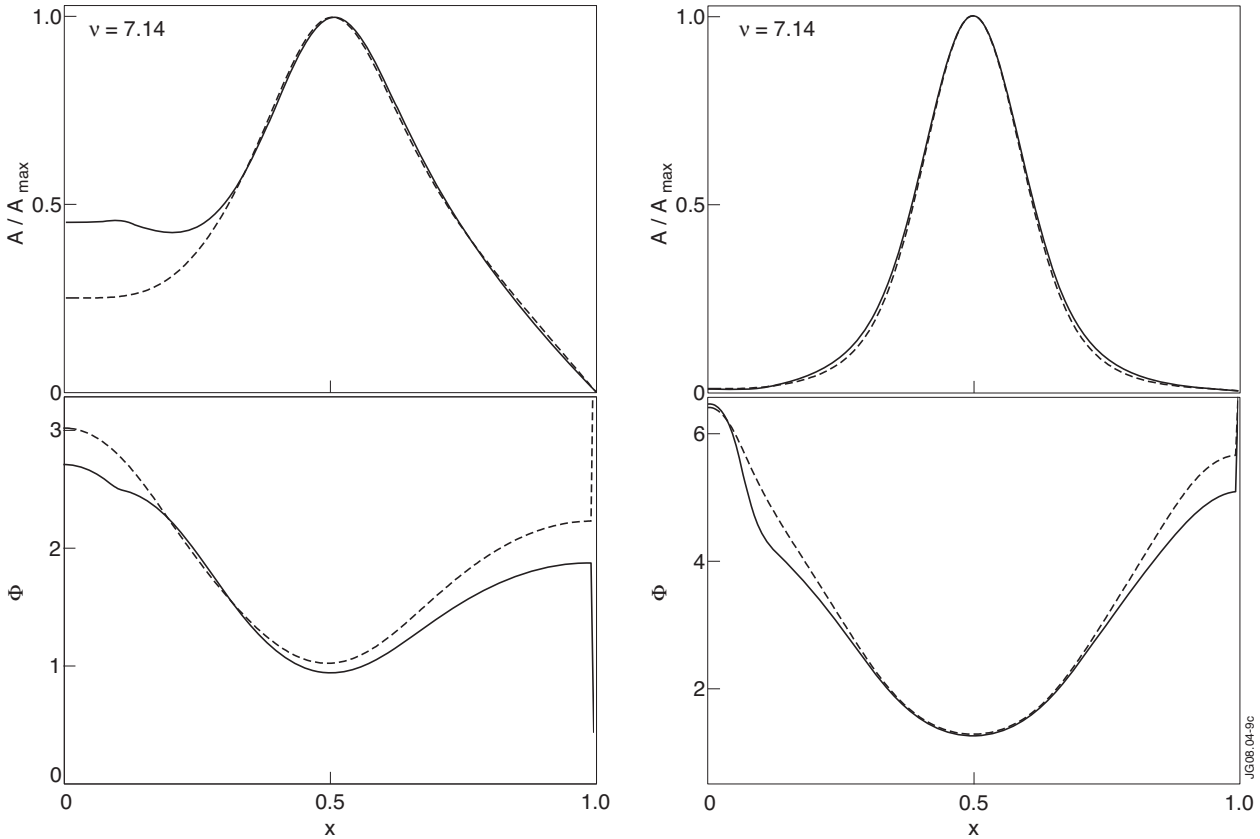

Figure 9: Dependence of the temperature perturbation, δT, in Eq. (16), on the non-locality parameter, α, and the frequency, ν, of the power modulation in Eq.(15). The figure shows the first harmonic of the normalized amplitude, $A_1(x)/A_{max}$, and phase, $\Phi_1(x)$, where $A_{max} = A_1(x = 1/2)$. The column on the left corresponds to the low frequency, ν = 7.14, perturbation, and the column on the right corresponds to the high frequency, ν = 57.14, perturbation. The solid line gives the result for $\alpha = 1.25$, and the dashed line corresponds to the standard, local diffusive response.

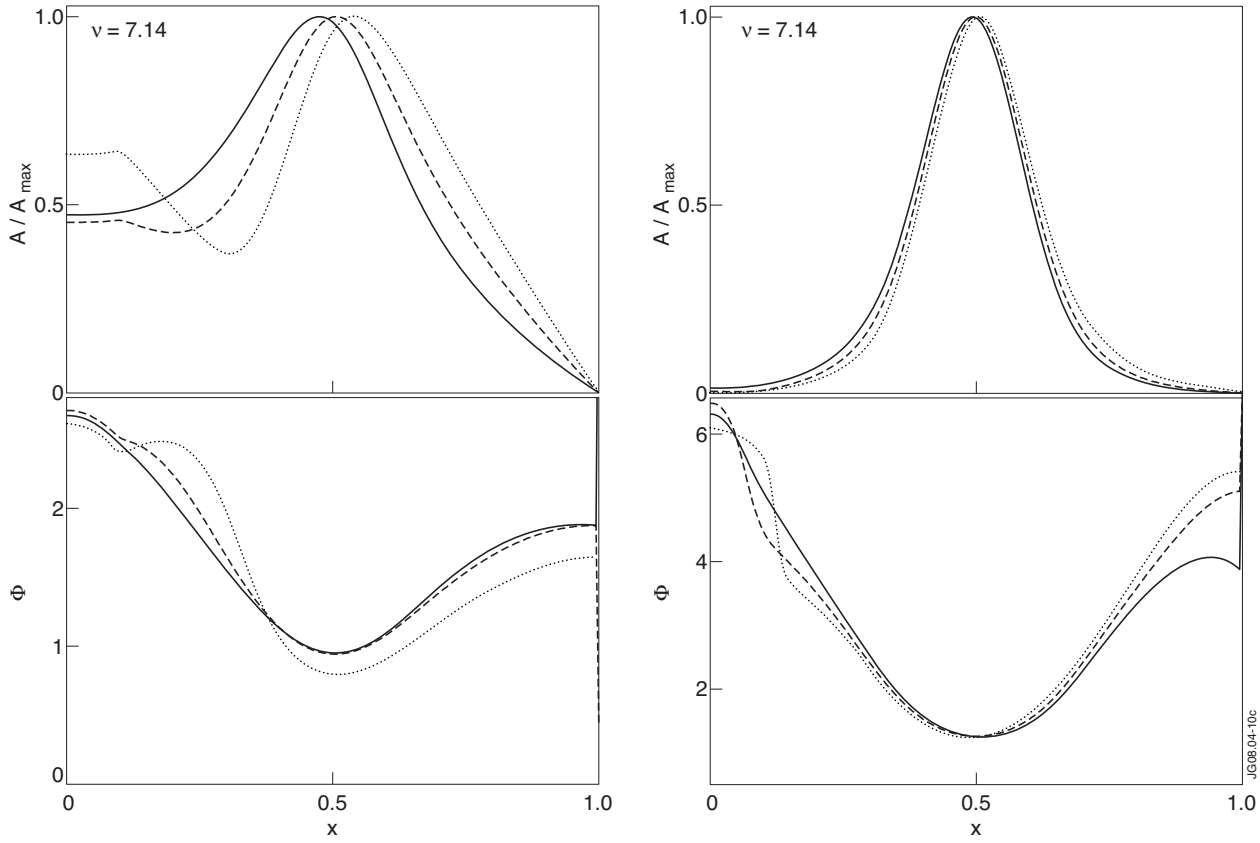

Figure 10: Dependence of the temperature perturbation, δT, in Eq.(16), on the asymmetry parameter, θ, and the frequency, ν, of the power modulation in Eq.(15). The figure shows the first harmonic of the normalized amplitude, $A_1(x)/A_{max}$, and phase, $\Phi_1(x)$, where $A_{max} = A_1(x = 1/2)$. The column on the left corresponds to the low frequency, ν = 7.14, perturbation, and the column on the right corresponds to the high frequency, ν = 57.14, perturbation. The solid line gives the result for θ = –1, the dashed line corresponds to θ = 0, and the dotted line corresponds to θ = 1.

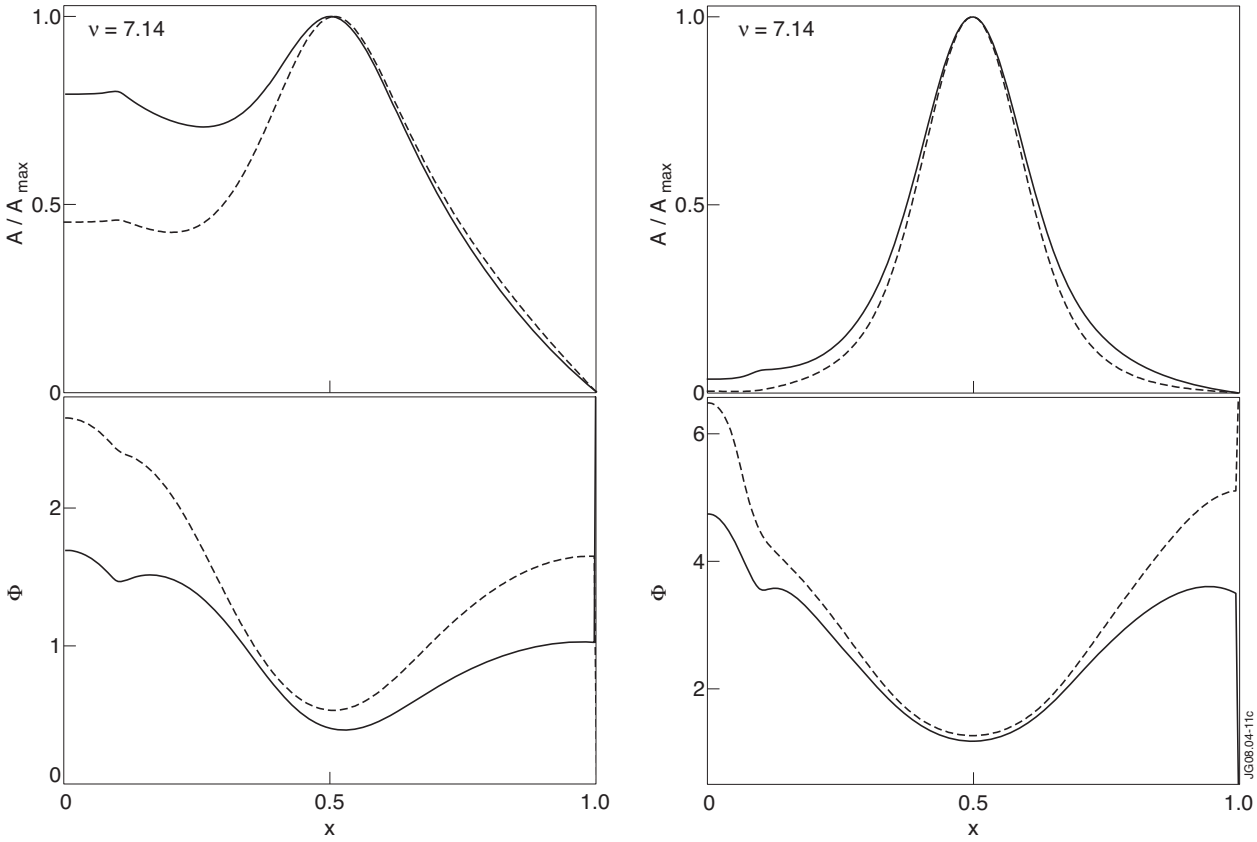

Figure 11: Dependence of the temperature perturbation, δT, in Eq.(16), on χ_s, and the frequency, ν, of the power modulation in Eq. (15). The figure shows the first harmonic of the normalized amplitude, $A_1(x)/A_{max}$, and phase, $\Phi_1(x)$, where $A_{max} = A_1(x = 1/2)$. The column on the left corresponds to the low frequency, ν = 7.14, perturbation, and the column on the right corresponds to the high frequency, ν = 57.14, perturbation. The solid line gives the result for $\chi_s = 5$, the dashed line corresponds to $\chi_s = 1$.

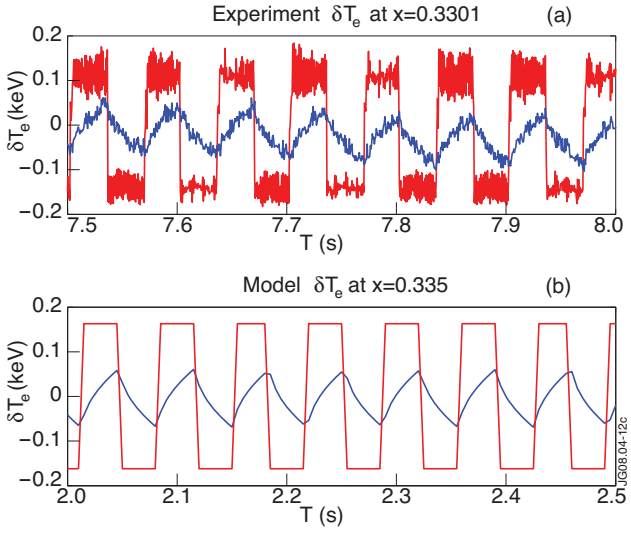

Figure 12. Traces of electron temperature perturbation and power modulation in JET (a) and in the fractional model (b). The square-wave periodic signal corresponds to the onoff power amplitude modulation, and the other signal corresponds to the electron temperature perturbation.

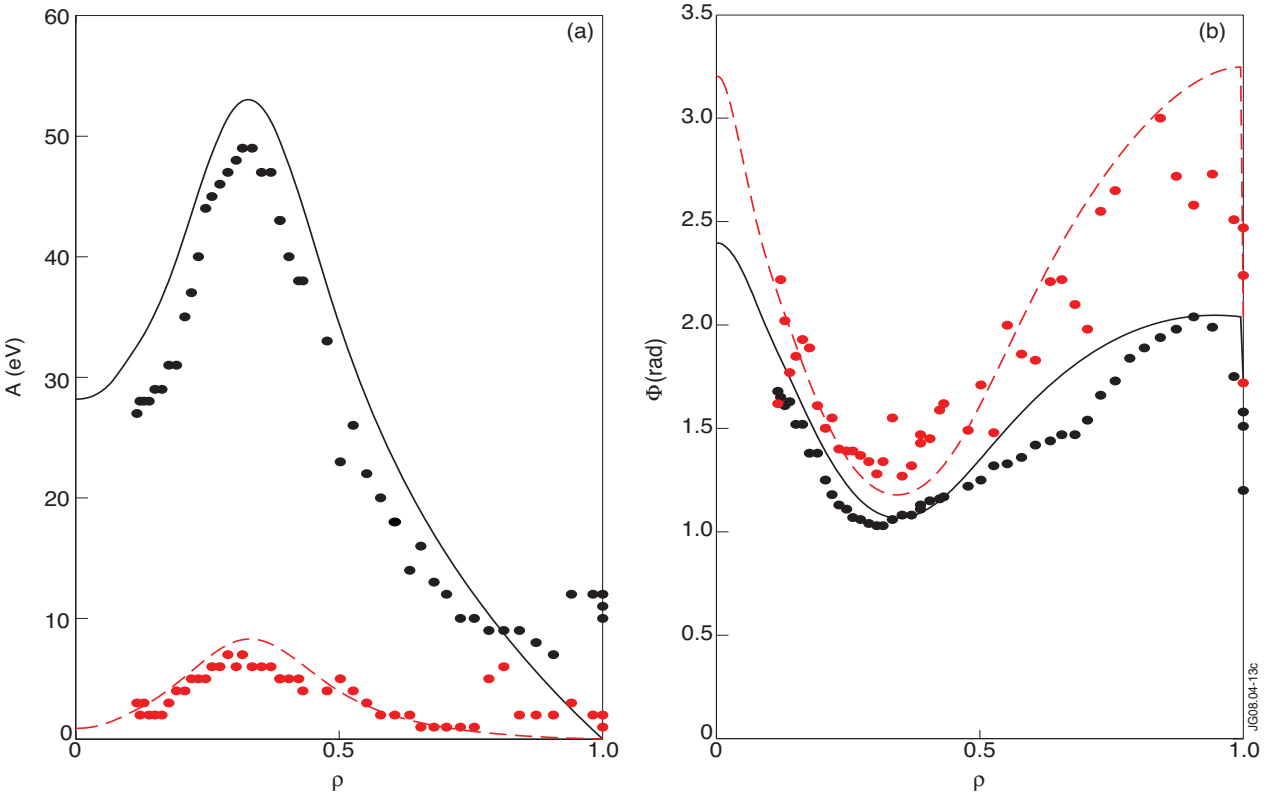

Figure 13. Experimental (dots) and fractional model (lines) profiles of the amplitude A *and phase delay* Φ *corresponding to the 1st (black) and the 3rd (red) Fourier harmonics of the electron temperature*

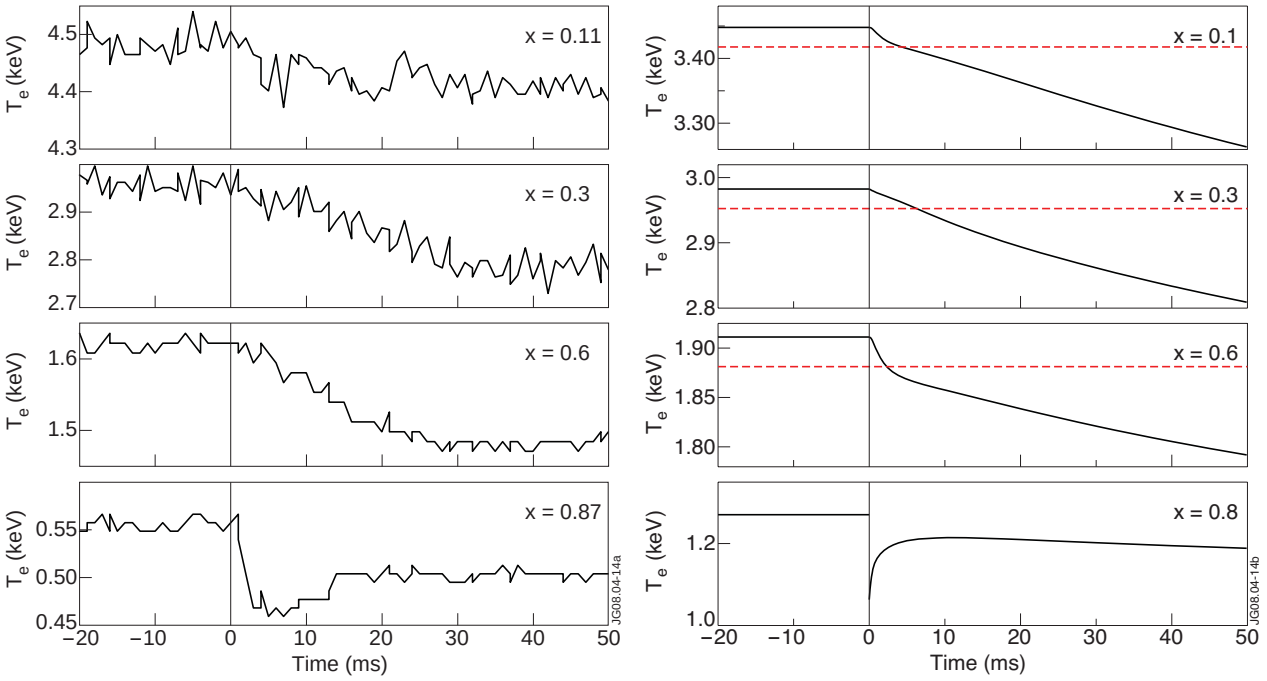

Figure 14. Comparison between the temperature traces in the experiment (left panel) and the model (right panel). Consistent with the experiment, the model exhibits a drop of 30eV (corresponding to the dashed red line) in about 4ms.